AMERICAN ACADEMY OF OPHTHALMOLOGY®

Deep Learning-based Quantification of Anterior Segment OCT Parameters

Zhi Da Soh, MPH,[1,2,] Mingrui Tan, BComp,[3,*] Monisha Esther Nongpiur, MD, PhD,[1,4] Marco Yu, PhD,[1,4] Chaoxu Qian, MD,[1] Yih Chung Tham, PhD,[1,2,5] Victor Koh, MD,[2,5] Tin Aung, MD, PhD,[1,2,4] Xinxing Xu, PhD,[3] Yong Liu, PhD,[3,**] Ching-Yu Cheng, MD, PhD[1,2,4,5,**]*

Objective: To develop and validate a deep learning algorithm that could automate the annotation of scleral spur (SS) and segmentation of anterior chamber (AC) structures for measurements of AC, iris, and angle width parameters in anterior segment OCT (ASOCT) scans.

Design: Cross-sectional study.

Subjects: Data from 2 population-based studies (i.e., the Singapore Chinese Eye Study and Singapore Malay Eye Study) and 1 clinical study on angle-closure disease were included in algorithm development. A separate clinical study on angle-closure disease was used for external validation.

Method: Image contrast of ASOCT scans were first enhanced with CycleGAN. We utilized a heat map regression approach with coarse-to-fine framework for SS annotation. Then, an ensemble network of U-Net, full resolution residual network, and full resolution U-Net was used for structure segmentation. Measurements obtained from predicted SSs and structure segmentation were measured and compared with measurements obtained from manual SS annotation and structure segmentation (i.e., ground truth).

Main Outcome Measures: We measured Euclidean distance and intraclass correlation coefficients (ICC) to evaluate SS annotation and Dice similarity coefficient for structure segmentation. The ICC, Bland–Altman plot, and repeatability coefficient were used to evaluate agreement and precision of measurements.

Results: For SS annotation, our algorithm achieved a Euclidean distance of 124.7 μm, ICC $\geq$ 0.95, and a 3.3% error rate. For structure segmentation, we obtained Dice similarity coefficient $\geq$ 0.91 for cornea, iris, and AC segmentation. For angle width measurements, $\geq$ 95% of data points were within the 95% limits-of-agreement in Bland–Altman plot with insignificant systematic bias (all $P > 0.12$). The ICC ranged from 0.71–0.87 for angle width measurements, 0.54 for IT750, 0.83–0.85 for other iris measurements, and 0.89–0.99 for AC measurements. Using the same SS coordinates from a human expert, measurements obtained from our algorithm were generally less variable than measurements obtained from a semiautomated angle assessment program.

Conclusion: We developed a deep learning algorithm that could automate SS annotation and structure segmentation in ASOCT scans like human experts, in both open-angle and angle-closure eyes. This algorithm reduces the time needed and subjectivity in obtaining ASOCT measurements.

Financial Disclosure(s): The author(s) have no proprietary or commercial interest in any materials discussed in this article.

Supplemental material available at www.ophthalmologyscience.org.

Primary angle-closure glaucoma (PACG) is a major cause of glaucoma-related blindness.[1] It is part of a spectrum of diseases known as primary angle-closure disease (PACD), where it is preceded in severity by primary angle-closure suspect (PACS) and primary angle-closure (PAC).[2] Although both PACS and PAC are often asymptomatic and nonsight threatening,[2] knowledge on the natural history of PACD progression or angle narrowing remains limited.[3] This may preclude timely detection of eyes at higher risk of disease progression for targeted interventions or closer monitoring.

As compared with gonioscopy, anterior segment OCT (ASOCT) provides a cross-sectional scan of the anterior chamber (AC) for qualitative appraisal and further allows for quantification of the angle space and its surrounding structures.[4] The latter enables monitoring of disease progression and evaluating the effectiveness of treatment such as laser iridotomy. However, ASOCT requires the manual annotation of the scleral spur (SS) for structure measurements, which is subjective and time-consuming to perform. This may hinder the use of ASOCT in clinical settings and is laborious for research

https://doi.org/10.1016/j.xops.2023.100360
ISSN 2666-9145/23

use. Furthermore, 15%−30% of SSs in ASOCT scans may be indiscernible to human graders,[5,6] with wide intra- and interassessor variability.[6,7] SS identification is further confounded by increased age,[8] brown irises,[9] and angle-closure.[6,9] This is unfortunate, given that the risk of PACD increases with age and in Asian adults, who tend to have darker irises and would benefit more from ASOCT assessment.

Nonetheless, the advents of artificial intelligence have provided multiple opportunities for value innovation. In PACD, deep learning (DL) algorithms have been developed to detect PACD from ASOCT scans via a binary classifier.[10,11] In addition, DL algorithms that could automate AC measurements in ultrasound biomicroscopy and Casia swept-source OCT images (Tomey Corporation) have also been reported.[12−14] However, such an algorithm has not been reported for use in other ASOCT modalities.

Hence, the aims of our study were two fold. We aimed to, first, develop and validate a DL algorithm that could automate SS annotation and segmentation of AC structures and, second, automate the measurements of AC, iris, and angle width in Visante ASOCT scans. This algorithm may provide a more consistent SS reference point and thus reduce the time needed to evaluate AC structures quantitatively, either in busy clinical or research settings.

Methods

This study was conducted at the Singapore Eye Research Institute. We obtained ethics approval from the SingHealth Centralized Institutional Review Board and conducted our study according to the tenets of the Declaration of Helsinki. Informed consent was obtained from all participants in the respective studies.

Study Population

First, we included participants from the Singapore Chinese Eye Study and Singapore Malay Eye Study, which are ongoing population-based cohort studies that recruit adults aged ≥40 years in Singapore. The detailed methodology for both studies has been described previously.[15] Briefly, an age-stratified random sampling was used to select participants living across the southwestern region of Singapore. We utilized data from baseline examinations, which were conducted from 2004−2006 in the Singapore Malay Eye Study (response rate, 78.7%) and from 2009−2011 in the Singapore Chinese Eye Study (response rate, 72.8%).

Second, we included participants enrolled in a clinical study (Iris and Choroidal Characteristics Study) that evaluated the pathomechanism of PACD.[16] This study was comprised of participants diagnosed with PACS, PAC, or PACG and those with a history of acute primary angle-closure with or without previous intraocular surgery. This study further included people with open angles, normal intraocular pressure (< 21 mmHg), and healthy optic nerve heads as normal controls, whereas those with secondary angle-closure (e.g., neovascular glaucoma) and inflammatory eye diseases (e.g., uveitis) were excluded.

Third, we included participants from an ongoing clinical study (Phenotyping Study) that evaluates the influence of genetic factors in PACG pathophysiology.[17] This study included participants diagnosed with PAC or PACG and excluded those with history of intraocular surgery, secondary angle-closure, and inflammatory eye diseases.

Study Examination

The procedure involved in ASOCT imaging and gonioscopy were similar in the included studies. First, ASOCT imaging was performed with Visante ASOCT (Carl Zeiss Meditec) in a dark room (≤ 5 lux) after dark adaption of 1 to 2 minutes. Before image capture, the refractive error of participants' eyes was entered into the system to reduce the amount of accommodation needed, which mitigates against excessive pupil constriction that may artificially widen the angle space. During image capture, the fixation target and patient head position were adjusted such that the temporal and nasal irises were aligned horizontally with minimal tilt. Images were centered on the pupil, and the reflex saturation beam was used to ensure scans were aligned along the visual axis. The upper and lower eyelids were gently retracted as needed for unobstructed image acquisition, with care taken to avoid inadvertent pressure on the globe. Images that were tilted, had poor clarity or alignment, were obscured by the eyelid, or were affected by motion artifacts were repeated, if possible. Otherwise, the assessor optimized the polarization of each scan and adjusted the image saturation and noise to obtain the best possible image quality.

Second, gonioscopy was performed by trained ophthalmologists under dim illumination. Static gonioscopy was performed with a Goldman 2-mirror gonioscope (Ocular Instruments Inc) at ×16 magnification. Dynamic gonioscopy was performed with a 4-mirror Sussman gonioscope (Ocular Instruments Inc) to assess for peripheral anterior synechiae in angles that seemed closed on static gonioscopy. During examination, care was taken to avoid light from falling on the pupil and minimize inadvertent indentation of the globe. The angle in each quadrant on gonioscopy was considered closed if the posterior trabecular meshwork was not observable in the primary position without indentation. This grading method has been reported in previous studies.[18,19] Eyes with ≥ 2 closed quadrants were diagnosed with PACD in our study.

Data Preparation

We utilized data from Singapore Chinese Eye Study, Singapore Malay Eye Study, and Iris and Choroidal Characteristics Study for algorithm development and internal testing and the Phenotyping Study data set for external testing. We appraised the quality of ASOCT images and excluded 162 images with clearly indiscernible SSs. Two investigators (M.N. and Z.D.S.) reached a consensus on the definition of the SS, and any disagreement was adjudicated by the senior author (C.-Y.C.). We defined the SS as the intersection point between the ciliary muscle and inner corneal margin or as a bump-like structure on the inner corneal meshwork margin.[9] We further defined the SS, when possible, as the most posterior end point of the trabecular corneoscleral surface[20] or at 1 mm posterior to the Schwalbe line along the internal corneal margin.[9] Both investigators annotated SSs in 60 Visante images (0°−180° angles) with the Zhongshan Angle Assessment Program (ZAAP) software for an agreement analysis.[21] These images were randomly selected by the study engineer (M.R.T.) from the algorithm training data set and were annotated by both investigators without the knowledge of gonioscopy findings. The intraclass correlation coefficients (ICCs) between both investigators for SS annotation were 0.99 in the x-axis and 0.97 in the y-axis.

Next, 2 investigators (C.Q. and Z.D.S.) reached a consensus on the boundaries of the iris, with any disagreement adjudicated by the senior author (C.-Y.C.). The outline of the iris at the angle space was first demarcated using Microsoft Paint and then segmented along with the corneoscleral shell and AC using the Medical Image

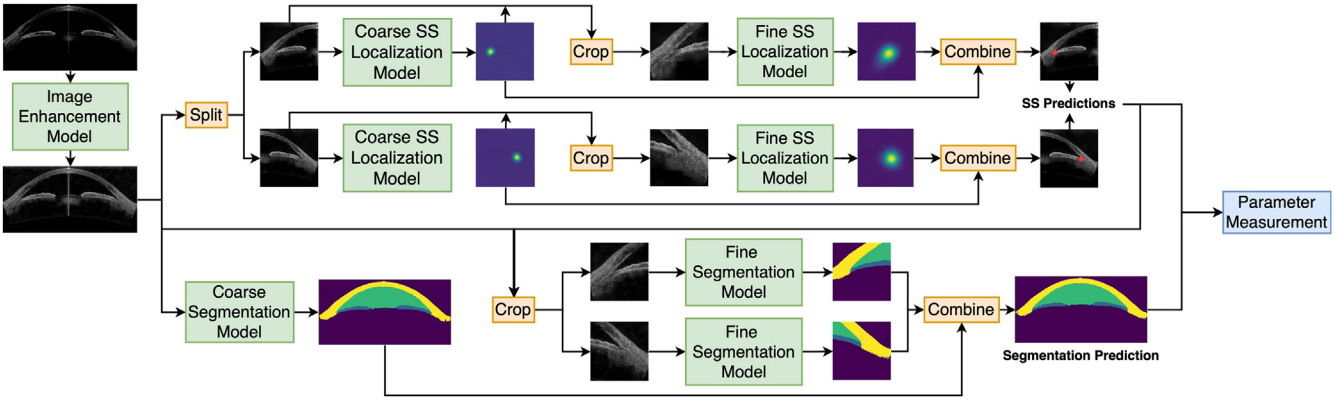

Figure 1. Deep learning developmental process for scleral spur localization, structure segmentation, and anterior segment OCT parameters measurements. SS = scleral spur.

Processing, Analysis, and Visualization software developed by the Center for Information Technology, National Institutes of Health.[22]

Algorithm Development and Testing

Image Enhancement Processing. First, we utilized CycleGAN to enhance the image contrast of Visante scans.[23] For this, we utilized the image-to-image translation CycleGAN model to translate Visante ASOCT images to Casia swept-source OCT images, which have higher resolution. As compared with traditional contrast enhancement techniques, such as intensity value mapping and histogram equalization, the CycleGAN model is a DL-based method that considers structural information of each image to provide output that closely resembles the Casia swept-source OCT images.

SS Annotation. Second, we adopted the heat map regression approach with coarse-to-fine framework for SS annotation.[24] The architecture used is a U-Net backbone with EfficientNet-B5 as the encoder for both coarse and fine models (Annex A, available at www.ophthalmologyscience.org). Each model performs regression against the ground truth heat maps obtained from human SS annotations. During training, the region of interest is randomly cropped around the initial prediction from coarse predicted heat map. During inference, the region of interest is directly centered on the initial prediction. The fine model takes the cropped region of interest as input and outputs the fine predicted heat map, which will generate the final SS location prediction.

ASOCT Structure Segmentation. Third, we adopted the architecture from our previous work, which comprised an ensemble network of U-Net, full resolution residual network, and full resolution residual U-Net for structure segmentation.[12] Each pixel in the image is classified into one of the following 4 classes: iris, corneosclera shell, AC, and the background. Each of the 3 models was trained individually, and the output from these models was used to train the ensemble network, which consists of a fully connected layer with rectified linear activation function,[25] a dropout layer with probability of 0.5, and a final fully connected layer with softmax activation function (Annex B, available at www.ophthalmologyscience.org).

ASOCT Parameter Measurements. Subsequently, we utilized the predicted SS annotation and structure segmentation to measure the following ASOCT parameters: angle opening distance (AOD), trabecular iris space area (TISA), iris thickness (IT), iris area, iris curvature, AC width, AC area, AC depth (ACD), and lens vault (LV). The definition of these parameters has been described previously.[4] We used image processing techniques to localize key points (e.g., extreme ends of the iris), and measure distances and areas to produce the parameter measurements. For iris area and AC area, we measured the area enclosed by the contour to reduce the effect of small segmentation errors within the iris or AC. The development process, starting from image enhancement processing to parameter measurement, is illustrated in Figure 1.

Hardware Specification. All models were trained and tested on an NVIDIA RTX 2080 Ti GPU with CUDA v11.0. For each ASOCT image, our algorithm annotated the SS in 0.419 seconds

Table 1. Demographic and Ocular Characteristics of Participants Included in Algorithm Development and Testing

	Training Data Set	Validation Data Set	Internal Testing Data Set	External Testing Data Set
Participants (N)	1536	219	440	164
Age, yrs (SD)	58.6 (9.0)	58.3 (9.4)	58.5 (9.2)	69.0 (8.9)
Sex, male (%)	726 (47.3)	116 (53.0)	219 (49.8)	63 (38.4)
Ethnicity, Chinese (%)	1341 (87.3)	181 (82.7)	398 (90.5)	151 (92.1)
Open angle, n, (%)*	1360 (74.6)	198 (73.9)	360 (67.4)	0 (0)
Angle closure, n (%)*	463 (25.4)	70 (26.1)	174 (32.6)	164 (100)

Notes: Data presented are mean (standard deviation) for continuous variables; frequency (percentage) for categorical variables.
ASOCT = anterior segment OCT; SD = standard deviation.
*One ASOCT scan per eye was included. Angle closure defined as ≥ 2 quadrants of occluded posterior trabecular meshwork on gonioscopy.

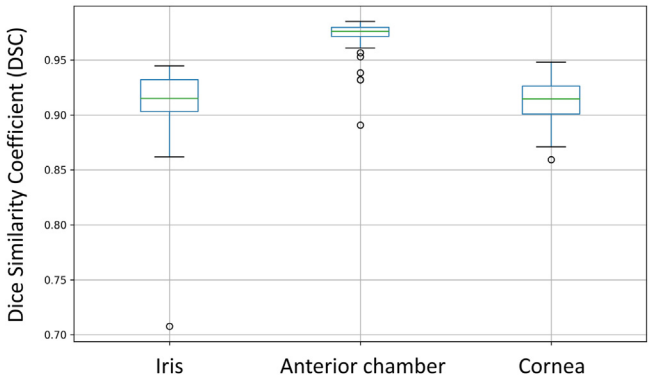

Figure 2. Agreement between ground truth and algorithm-predicted segmentation masks in internal testing.

and segmented AC structures in 0.436 seconds on average. ASOCT parameters were measured on an Intel Xeon W-2295 CPU at 3.0 GHz in 2.21 seconds on average.

Statistical Analysis. The ground truth for SS cartesian point and structure segmentation was established based on manual annotation of ASOCT images by experienced graders (Z.D.S. and M.N.). First, to evaluate the accuracy of SS localization, we measured the Euclidean distance between ground truth and algorithm-predicted SSs with the formula: $\sqrt{}$ ([X-coordinate difference]^2 + [Y-coordinate difference]^2). We further evaluated the relative agreement between ground truth and algorithm-predicted SSs with the 2-way, single score, absolute agreement ICC model and defined values < 0.50 as poor, 0.50 to < 0.75 as moderate, 0.75 to 0.90 as good, and > 0.90 as excellent reliability.[26,27] Second, to evaluate the accuracy of structure segmentation, we compared the relative agreement between ground truth and algorithm segmentations with the Dice similarity coefficient (DSC), which ranges from 0 (no overlap) to 1 (perfect overlap or agreement).[28]

Third, we evaluated the effect of deviation in algorithm-predicted SS localization and structure segmentation on subsequent ASOCT measurements. For this, we utilized the ICC, repeatability coefficients (RCs) and Bland–Altman plot to compare the agreement and level of precision between ASOCT measurements obtained using ground truth SS and structure segmentation (i.e., ground truth measurements) with ASOCT measurements obtained using algorithm-predicted SS and structure segmentation (i.e., algorithm measurements). Both sets of measurements were obtained using the measurement codes from our DL algorithm.

Fourth, we utilized the ICCs and RCs to evaluate the agreement and level of precision between ground truth measurements and measurements obtained using the ZAAP software (i.e., ZAAP measurements). The ZAAP measurements utilized ground truth SS, ZAAP structure segmentation, and ZAAP measurement codes. All statistical analyses were performed using Python (V3.8, Tensorflow 2.7.0, PaddlePaddle 1.8.5).

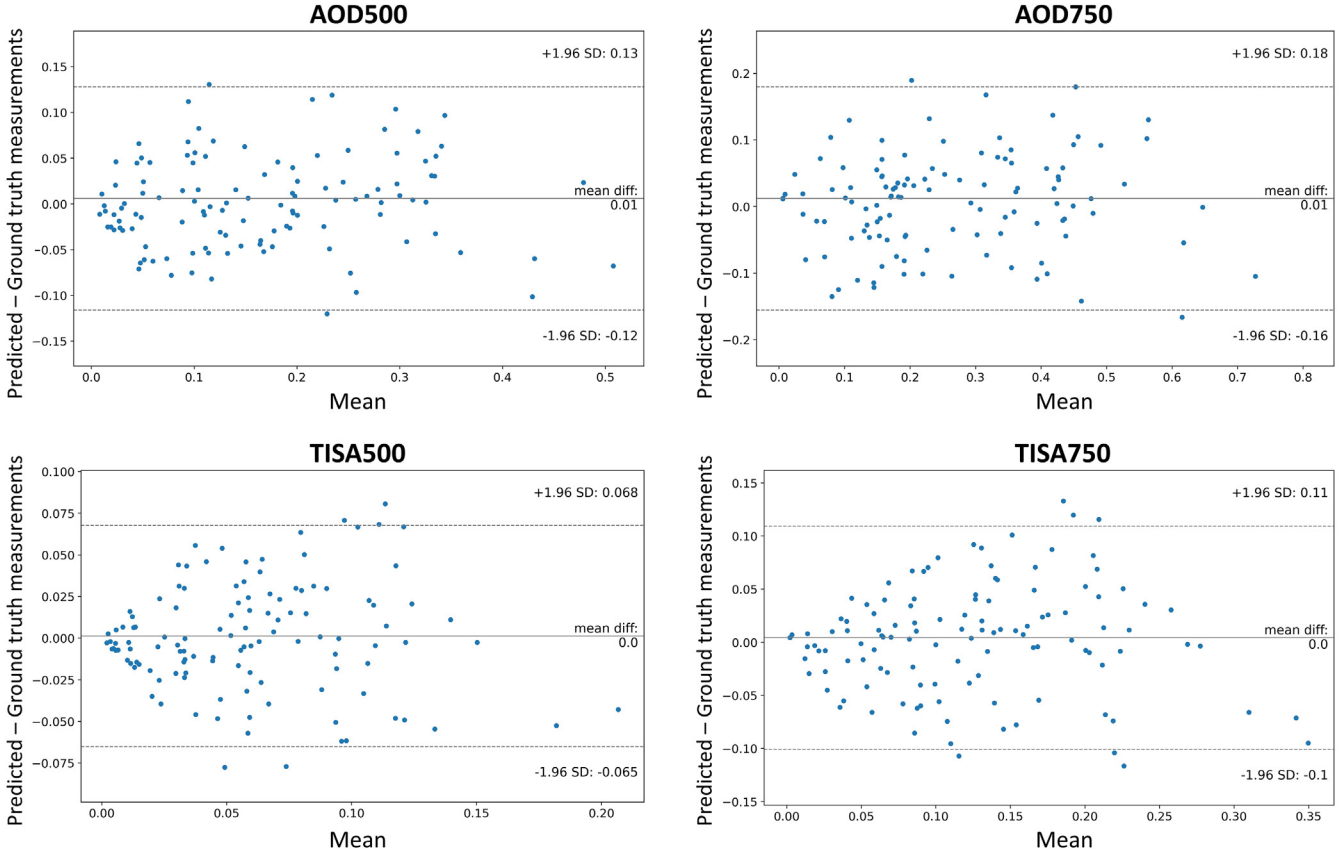

Figure 3. Bland–Altman plots illustrating the agreement between predicted and ground truth angle measurements in internal testing. AOD = angle opening distance; TISA = trabecular iris space area.

Table 3. Intraclass Correlation and Repeatability Coefficients of Measurements Obtained from Deep Learning Algorithm as Compared with Ground Truth Measurements in Internal Testing

	Overall (N = 120)*		Open angle (n = 51)		Angle closure (n = 69)	
ASOCT parameters	*ICC*	*RC*	*ICC*	*RC*	*ICC*	*RC*
AOD500	0.87	0.17	0.81	0.21	0.81	0.14
AOD750	0.87	0.24	0.82	0.28	0.83	0.20
TISA500	0.71	0.09	0.64	0.11	0.60	0.08
TISA750	0.79	0.15	0.71	0.18	0.72	0.12
IT750	0.54	0.18	0.49	0.19	0.59	0.17
IT2000	0.83	0.12	0.83	0.12	0.84	0.12
I-Area	0.85	0.32	0.90	0.25	0.80	0.36
I-Curv	0.85	0.16	0.76	0.17	0.88	0.16
ACD	0.89	0.43	0.89	0.38	0.88	0.46
ACA	0.99	1.01	0.99	1.35	0.99	0.66
ACW	0.93	0.37	0.84	0.49	0.97	0.24
LV	0.93	0.32	0.85	0.42	0.96	0.21

ACA = anterior chamber area; ACD = anterior chamber depth; ACW = anterior chamber width; AOD = angle opening distance; ASOCT = anterior segment OCT; I-Area = iris area; ICC = intraclass correlation coefficient; I-Curv = iris curvature; IT = iris thickness; LV, lens vault; RC = repeatability coefficient; SS = scleral spur; TISA = trabecular iris space area.
*Ground truth measurements obtained using SS annotation and structure segmentation by trained grader and algorithm measurement codes. Algorithm measurements obtained using algorithm-predicted SS and structure segmentation and algorithm measurement codes. 60 scans of 60 eyes were selected; each scan was divided into 2 (left and right side), resulting in 120 measurements (51 open angles; 69 angle closure based on gonioscopy grading).

Results

We included 2195 participants in the training, validation, and internal testing of our DL algorithm (Table 1). This comprised of 2625 eyes, of which 26.9% were diagnosed with angle closure. In the internal test data set, 534 eyes (534 scans) were used to evaluate the algorithm performances in SS localization and structure segmentation, of which 60 eyes were randomly selected to evaluate the agreement between ground truth and algorithm measurements. We further included another 164 eyes with angle closure for external testing.

Table 4. Intraclass Correlation and Repeatability Coefficients of Measurements Obtained from the Zhongshan Angle Assessment Program (ZAAP)

	ZAAP (N = 120)*	
ASOCT Parameters	*ICC*	*RC*
AOD500	0.88	0.16
AOD750	0.81	0.27
TISA500	0.64	0.11
TISA750	0.73	0.16
IT750	0.02	0.50
IT2000	0.28	0.45
I-Area	0.29	1.44
I-Curv	0.31	0.57
ACD	0.99	0.15
ACA	0.93	3.70
ACW	0.96	0.28
LV	0.96	0.25

ACA = anterior chamber area; ACD = anterior chamber depth; ACW = anterior chamber width; AOD = angle opening distance; ASOCT = anterior segment OCT; I-Area = iris area; ICC = intraclass correlation coefficient; I-Curv = iris curvature; IT = iris thickness; LV = lens vault; RC = repeatability coefficient; SS = scleral spur; TISA = trabecular iris space area; ZAAP = Zhongshan Angle Assessment Program.
*Ground truth measurements obtained using SS annotation and structure segmentation by trained grader and algorithm measurement codes. ZAAP measurements obtained using SS annotation by trained grader and ZAAP structure segmentation and measurement codes. Sixty scans of 60 eyes were selected; each scan was divided into 2 (left and right side), resulting in 120 measurements.

In internal testing, the average Euclidean distance between algorithm- and human-annotated SSs was 4.66 pixels or 124.74 μm. The ICC between algorithm- and human-annotated SSs was 0.99 on the x-axis and between 0.95−0.98 on the y-axis (Table S2, available at www.ophthalmologyscience.org). Overall, the DSCs for cornea, iris, and AC structures were 0.91, 0.91, and 0.97, respectively (Fig 2). The DSCs for cornea, iris, and AC structures were 0.92, 0.92, and 0.97, respectively, in eyes with open angles and 0.91, 0.91, and 0.97, respectively, in eyes with angle closure.

The Bland−Altman plot for angle width measurements (AOD and TISA) is presented in Figure 3, whereas plots for iris (Fig S4, available at www.ophthalmologyscience.org) and AC measurements (Fig S5, available at www.ophthalmologyscience.org) are included in supplementary materials. For angle measurements, $\geq$ 95% of data points were within the 95% limits-of-agreement with insignificant systematic bias (all $P > 0.12$). A significant but weak proportional bias was observed for AOD500 ($r = 0.20$, $P = 0.03$) and AOD750 ($r = 0.20$, $P = 0.02$) but not TISA500 ($r = 0.07$, $P = 0.422$) and TISA750 ($r = 0.10$, $P = 0.282$). However, higher variance was observed in larger TISA measurements as compared with AOD (Fig 3).

Compared with ground truth measurements, algorithm measurements achieved ICC between 0.71−0.87 for angle width measurements and between 0.89−0.99 for AC measurements (Table 3). The ICC for IT750 was 0.54 and

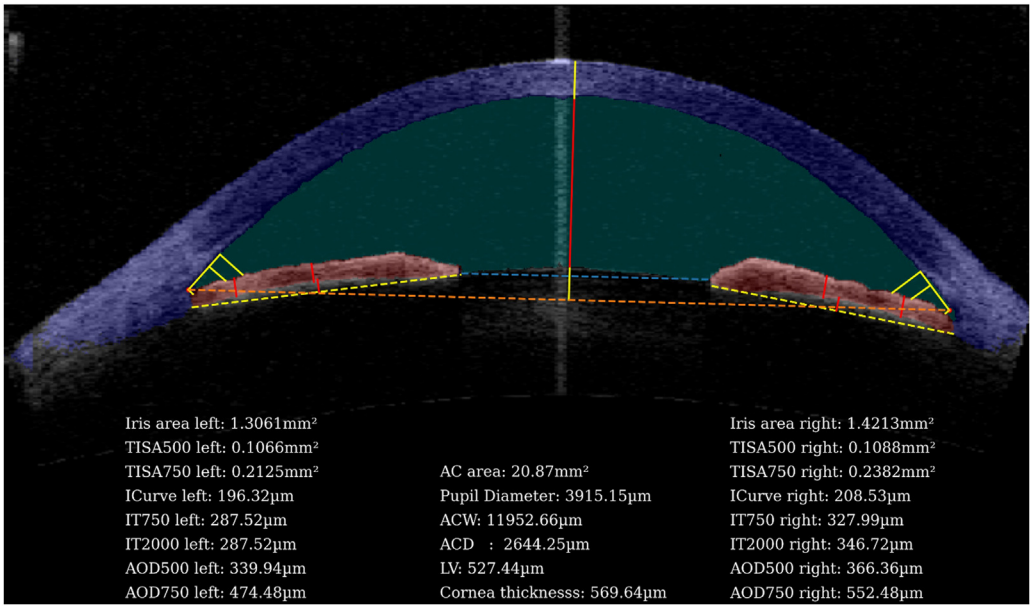

Figure 8. Example of scleral spur annotation, structure segmentation, and measurements by deep learning algorithm. AC = anterior chamber; ACD = anterior chamber depth; ACW = anterior chamber width; AOD, angle opening distance; ICC = intraclass correlation coefficient; I-Curv = iris curvature; IT = iris thickness; LV, lens vault; TISA = trabecular iris space area.

ranged between 0.83−0.85 for other iris measurements. The ICC values for angle width, AC, and iris measurements were similar in eyes with open angles and angle closure (Table 3). In addition, the RCs for all measurements, except iris area and ACD, were lower in eyes with angle closure (Table 3). In contrast, ZAAP achieved ICC between 0.64−0.88 for angle width measurements and between 0.93−0.99 for AC measurements (Table 4). The ICC for IT750 was 0.02 and ranged between 0.28−0.31 for other iris measurements. As compared with our DL algorithm measurements, the RCs for AOD500, TISA500/750, all iris measurements, and AC area were higher (i.e., less precise) in measurements obtained from ZAAP (Table 4).

Manual inspection on algorithm-predicted SS annotations and structure segmentation in internal testing showed 4 errors (3.3%) in SS annotation (Fig S6, available at www.ophthalmologyscience.org), whereas 9 images had segmentation error in the AC, including 1 with additional iris segmentation error (Fig S7, available at www.ophthalmologyscience.org). After removing the 4 cases of erroneous SS annotations, the ICC for angle measurements remained similar (Table S5, available at www.ophthalmologyscience.org). After removing the 9 cases of erroneous segmentations, the ICC for ACD improved marginally from 0.93−0.96m whereas the ICC for LV improved from 0.93−0.95.

In external testing, the average Euclidean distance between algorithm- and human-annotated SSs was 5.1 pixels or 136.36 µm. The ICCs between algorithm- and human-annotated SSs were 0.99 on the x-axis and between 0.96 on the y-axis. The mean DSCs for cornea, iris, and AC structures were 0.88, 0.91, and 0.97, respectively. Manual inspection showed 5 (4.2%) errors in SS annotation, 2 (1.7%) in AC segmentation, and 3 (2.5%) in iris segmentation.

Discussion

In this study, we developed a DL algorithm that could automate the measurements of AC structures in Visante ASOCT images (Fig 8). This DL algorithm performed on par with experienced graders, including a glaucoma specialist, with few errors in SS annotation (3 in 100 cartesian points) and segmentation (3 in 20 images) in internal testing. Measurements from our algorithm were generally less variable than measurements obtained from ZAAP, especially for iris parameters. Importantly, measurements obtained in eyes with angle closure were similar, if not less variable, than eyes with open angles.

Quantitative measurements from ASOCT may complement gonioscopy in the clinical assessment of PACD. As compared with gonioscopy, these measurements are better correlated with IOP,[29] are more predictive of PACD development and progression,[30,31] and may aid in prognosticating the effect of laser peripheral iridotomy.[32] However, the need for manual SS annotation has, in part, limited the routine use of ASOCT in clinics and is laborious for use in research studies.

To mitigate this, we developed a DL algorithm to automate the process of obtaining measurements from ASOCT scans. This algorithm was trained with SS annotations provided by trained graders and based on a broad definition of SS. We utilized a combination of 4 SS definitions to account for the wide variation in its appearances. Seager et al[9] reported that a combination of 3 of these definitions

could accurately identify 98% of all SSs. Furthermore, algorithm-predicted SSs were close to annotations made by trained graders, with few errors in both internal (3.3%) and external testing (4.2%). This is important in mitigating variation in manual SS annotation, which may account for 50% of variability in TISA measurements.[21]

In addition, we utilized convolutional neural network to locate the SS and delineate ocular structures in ASOCT images via DL. Previous studies showed that DL algorithms outperformed traditional machine learning algorithms in the detection of PACD,[33,34] and performed well in automating ASOCT measurements in ultrasound biomicroscopy[14] and Casia swept-source OCT.[12] We utilized a coarse-to-fine framework to zoom in on the angle space and further utilized CycleGAN to enhance image contrast for better delineation of the angle space and SS identification. As a result, structure segmentation by our algorithm was similar to manual segmentation by human assessors in eyes, with different angle status in both internal and external testing (DSC $\geq$ 0.88).

Furthermore, measurements obtained from our algorithm were generally less variable than those obtained with ZAAP using the same SS coordinates and structure segmentation, especially for iris parameters. The ZAAP, a widely used program for obtaining Visante ASOCT measurements, utilizes differences in pixel intensity to delineate the boundaries of AC structures, which may be more difficult in eyes with angle closure due to the close proximity or contact between 2 highly reflective structures (i.e., iris and cornea).[6] This may result in wider variability and deviation in structure segmentation, especially for iris parameters and, thus, affects the repeatability of measurements.

Importantly, measurements obtained from our algorithm were similar or less variable in eyes with angle closure than in eyes with open angle. This may indicate robust structure segmentation and SS annotation in eyes with different angle status, which is helpful given that SS annotation has been reported to be more challenging in eyes with angle closure.[9] Alternatively, this may in-part be due to the peripheral iris being more parallel to the posterior corneal surface in eyes with angle closure and, as a result, is less sensitive or affected less by variation in SS annotation.[6]

Our algorithm is notable for the following reasons. Our algorithm was trained and tested with images obtained from different population-based studies, along with images of eyes with angle closure from different clinical studies. Thus, the included data set likely comprises a wide variety of angle configurations, which could improve the generalizability of our algorithm (although this requires further external testing). However, our algorithm is not without limitations. First, ground truth labels used in algorithm development came from 2 human assessors. Including more assessors would be helpful in balancing out the biases that a DL algorithm may mimic from any particular assessor. However, we attempted to mitigate this by adopting a broad definition of SS for our ground truth labeling and following the labels provided by an experienced glaucoma specialist. Second, comparison to previously published algorithms showed that our algorithm performed worse in SS annotation (i.e., higher Euclidean distance).[12,13] However, previous algorithms were developed using images from swept-source ASOCT, which has much better image resolution compared with Visante ASOCT. Third, Visante ASOCT was recently removed from the commercial market. However, studies that utilized Visante ASOCT previously (especially population-based studies) may still benefit from automated measurements of their data. Also, our algorithm may serve as a foundation for transfer learning to other ASOCT modalities.

In conclusion, we developed a DL algorithm that could automate the annotation of SSs and segmentation of AC structures in ASOCT scans like experienced graders, in both open-angle and angle-closure eyes. Measurements obtained from our algorithm were generally less variable than measurements obtained from ZAAP, especially for iris parameters. This algorithm is intended to reduce the time needed and subjectivity involved in obtaining ASOCT measurements.

Footnotes and Disclosures

Originally received: March 30, 2023.
Final revision: June 22, 2023.
Accepted: June 26, 2023.
Available online: July 3, 2023. Manuscript no. XOPS-D-23-00006R1.

[1] Singapore Eye Research Institute, Singapore National Eye Centre, Singapore.

[2] Department of Ophthalmology, Yong Loo Lin School of Medicine, National University of Singapore, Singapore.

[3] Institute of High Performance Computing, Agency for Science, Technology and Research, Singapore.

[4] Ophthalmology & Visual Sciences Academic Clinical Program, Duke-NUS Medical School, Singapore.

[5] Centre for Innovation and Precision Eye Health, Yong Loo Lin School of Medicine, National University of Singapore, Singapore.

*Z.D.S. and M.T. contributed equally as first authors.

**Y.L. and C.-Y.C contributed equally as last authors.

Disclosure(s):

All authors have completed and submitted the ICMJE disclosures form.

The author(s) have made the following disclosure(s):

This study was funded by the National Medical Research Council, Singapore (NMRC/CIRG/1442/2016 and NMRC/CIRG/1488/2018), and the Agency for Science, Technology and Research (A*Star) AME Programmatic Funds (A20H4b0141).

HUMAN SUBJECTS: Human subjects were included in this study. We obtained ethics approval from the SingHealth Centralized Institutional Review Board (CIRB) and conducted our study according to the tenets of the Declaration of Helsinki. Informed consent was obtained from all participants in the respective studies.

No animal subjects were used in this study.

Author Contributions:

Conception and design: Soh, Xu, Liu, Cheng

Data collection: Soh, Tan, Nongpiur

Analysis and interpretation: Soh, Tan, Yu

Obtained funding: Cheng, Liu

Overall responsibility: Soh, Tan, Nongpiur, Yu, Qian, Tham, Koh, Aung, Xu, Liu, Cheng

Abbreviations and Acronyms:
AC = anterior chamber; **ACD** = anterior chamber depth; **AOD** = angle opening distance; **ASOCT** = anterior segment OCT; **DL** = deep learning; **DSC** = Dice similarity coefficient; **ICC** = intraclass correlation coefficients; **IT** = iris thickness; **PAC** = primary angle-closure; **PACD** = primary angle-closure disease; **PACG** = primary angle-closure glaucoma; **PACS** = primary angle-closure suspect; **RC** = repeatability coefficient; **SS** = scleral spur; **TISA** = trabecular iris space area; **ZAAP** = Zhongshan Angle Assessment Program.

Keywords:
Angle closure, Anterior chamber measurements, Anterior segment OCT (ASOCT), Deep learning, Visante ASOCT.

Correspondence:
Ching-Yu Cheng, MD, PhD, Singapore Eye Research Institute, The Academia, Discovery Tower level 6, 20 College Road, Singapore 169856. E-mail: chengyu.cheng@duke-nus.edu.sg.

References

1. Friedman DS, Foster PJ, Aung T, He M. Angle closure and angle-closure glaucoma: what we are doing now and what we will be doing in the future. *Clin Exp Ophthalmol*. 2012;40:381−387.
2. Foster PJ, Buhrmann R, Quigley HA, Johnson GJ. The definition and classification of glaucoma in prevalence surveys. *Br J Ophthalmol*. 2002;86:238−242.
3. Teo ZL, Soh ZD, Tham YC, et al. Six-year incidence and risk factors for primary angle-closure disease: the Singapore Epidemiology of Eye Diseases Study. *Ophthalmology*. 2022;129:792−802.
4. Chansangpetch S, Rojanapongpun P, Lin SC. Anterior segment imaging for angle closure. *Am J Ophthalmol*. 2018;188:xvi−xxix.
5. Kim DY, Sung KR, Kang SY, et al. Characteristics and reproducibility of anterior chamber angle assessment by anterior-segment optical coherence tomography. *Acta Ophthalmol*. 2011;89:435−441.
6. Sakata LM, Lavanya R, Friedman DS, et al. Assessment of the scleral spur in anterior segment optical coherence tomography images. *Arch Ophthalmol*. 2008;126:181−185.
7. Tan AN, Sauren LD, de Brabander J, et al. Reproducibility of anterior chamber angle measurements with anterior segment optical coherence tomography. *Invest Ophthalmol Vis Sci*. 2011;52:2095−2099.
8. Liu S, Li H, Dorairaj S, et al. Assessment of scleral spur visibility with anterior segment optical coherence tomography. *J Glaucoma*. 2010;19:132−135.
9. Seager FE, Wang J, Arora KS, Quigley HA. The effect of scleral spur identification methods on structural measurements by anterior segment optical coherence tomography. *J Glaucoma*. 2014;23:e29−e38.
10. Fu H, Baskaran M, Xu Y, et al. A deep learning system for automated angle-closure detection in anterior segment optical coherence tomography images. *Am J Ophthalmol*. 2019;203:37−45.
11. Xu BY, Chiang M, Chaudhary S, et al. Deep learning classifiers for automated detection of gonioscopic angle closure based on anterior segment OCT images. *Am J Ophthalmol*. 2019;208:273−280.
12. Pham TH, Devalla SK, Ang A, et al. Deep learning algorithms to isolate and quantify the structures of the anterior segment in optical coherence tomography images. *Br J Ophthalmol*. 2021;105:1231−1237.
13. Xu BY, Chiang M, Pardeshi AA, Moghimi S, Varma R. Deep neural network for scleral spur detection in anterior segment OCT images: the Chinese American eye study. *Transl Vis Sci Technol*. 2020;9:18.
14. Wang W, Wang L, Wang X, et al. A deep learning system for automatic assessment of anterior chamber angle in ultrasound biomicroscopy images. *Transl Vis Sci Technol*. 2021;10:21.
15. Majithia S, Tham YC, Chee ML, et al. Cohort profile: the Singapore epidemiology of eye diseases study (SEED). *Int J Epidemiol*. 2021;50:41−52.
16. Chua J, Thakku SG, Tun TA, et al. Iris crypts influence dynamic changes of iris volume. *Ophthalmology*. 2016;123:2077−2084.
17. Nongpiur MEMD, He MMDP, Amerasinghe NM, et al. Lens vault, thickness, and position in Chinese subjects with angle closure. *Ophthalmology*. 2011;118:474−479.
18. Leung CKS, Cheung CYL, Li H, et al. Dynamic analysis of dark-light changes of the anterior chamber angle with anterior segment OCT. *Invest Ophthalmol Vis Sci*. 2007;48:4116−4122.
19. Baskaran MDNB, Iyer JVMM, Narayanaswamy AK, et al. Anterior segment imaging predicts incident gonioscopic angle closure. *Ophthalmology*. 2015;122:2380−2384.
20. Usui T, Tomidokoro A, Mishima K, et al. Identification of Schlemm's canal and its surrounding tissues by anterior segment fourier domain optical coherence tomography. *Invest Ophthalmol Vis Sci*. 2011;52:6934−6939.
21. Console JW, Sakata LM, Aung T, Friedman DS, He M. Quantitative analysis of anterior segment optical coherence tomography images: the Zhongshan Angle Assessment Program. *Br J Ophthalmol*. 2008;92:1612−1616.
22. McAuliffe MJ, Lalonde FM, McGarry D, et al. *Medical image processing, analysis and visualization in clinical research. Proceedings 14th IEEE Symposium on Computer-Based Medical Systems*. Bethesda, MD: CBMS 2001; 2001: 381−386. https://doi.org/10.1109/CBMS.2001.941749.
23. Zhu JY, Park T, Isola P, Efros AA. *Unpaired image-to-image translation using cycle-consistent adversarial networks. Paper presented at: 2017 IEEE International Conference on Computer Vision (ICCV)*, 22-29 October 2017. Venice: Italy; 2017: 2242−2251. https://doi.org/10.1109/ICCV.2017.244.
24. Fu H, Li F, Sun X, et al. AGE challenge: angle closure glaucoma evaluation in anterior segment optical coherence tomography. *Med Image Anal*. 2020;66:101798.
25. Xu B, Wang N, Chen T, Li M. *Empirical evaluation of rectified activations in convolutional network*. 2015:150500853. https://doi.org/10.48550/arXiv.1505.00853. *arXiv*.
26. Portney LG, Watkins MP. *Foundations of Clinical Research: Applications to Practice*. 892. Upper Saddle River, NJ: Pearson/Prentice Hall; 2009.
27. Koo TK, Li MY. A guideline of selecting and reporting intraclass correlation coefficients for reliability research. *J Chiropr Med*. 2016;15:155−163.
28. Guindon B, Zhang Y. Application of the Dice coefficient to accuracy assessment of object-based image classification. *Can J Remote Sens*. 2017;43:48−61.

29. Xu BY, Burkemper B, Lewinger JP, et al. Correlation between intraocular pressure and angle configuration measured by OCT: the Chinese American eye study. *Ophthalmol Glaucoma*. 2018;1:158−166.
30. Nongpiur ME, Aboobakar IF, Baskaran M, et al. Association of baseline anterior segment parameters with the development of incident gonioscopic angle closure. *JAMA Ophthalmol*. 2017;135:252−258.
31. Xu BY, Friedman DS, Foster PJ, et al. Ocular biometric risk factors for progression of primary angle closure disease: the Zhongshan Angle Closure Prevention Trial. *Ophthalmology*. 2022;129:267−275.
32. Xu BY, Friedman DS, Foster PJ, et al. Anatomic changes and predictors of angle widening after laser peripheral iridotomy: the Zhongshan Angle Closure Prevention Trial. *Ophthalmology*. 2021;128:1161−1168.
33. Fu H, Xu Y, Lin S, et al. Angle-closure detection in anterior segment OCT based on multilevel deep network. *IEEE Trans Cybern*. 2020;50:3358−3366.
34. Fu H, Xu Y, Lin S, et al. Multi-context deep network for angle-closure glaucoma screening in anterior segment OCT. Paper presented at: International Conference on Medical image computing and computer-assisted intervention - MICCAI 2018. September *Granada, Spain*. 2018:16−20.